Biogeosciences
Discussions

Open Access

EGU

1 **Global trends in marine nitrate N isotopes from observations and a neural network-**
2 **based climatology**
3
4 Patrick A. Rafter[1], Aaron Bagnell[2], Dario Marconi[3], and Timothy DeVries[2]
5
6 1: University of California, Irvine; 2 University of California, Santa Barbara; 3: Princeton
7 University
8
9 **Abstract**
10 Nitrate is a critical ingredient for life in the ocean because, as the most abundant form of
11 fixed nitrogen in the ocean, it is an essential nutrient for primary production. The
12 availability of marine nitrate is principally determined by biological processes, each having
13 a distinct influence on the N isotopic composition of nitrate (nitrate δ^{15}N)—a property that
14 informs much of our understanding of the marine N cycle as well as marine ecology,
15 fisheries, and past ocean conditions. However, the sparse spatial distribution of nitrate δ^{15}N
16 observations makes it difficult to apply this useful property in global studies, or to facilitate
17 robust model-data comparisons. Here, we use a compilation of published nitrate δ^{15}N
18 measurements (n = 12277) and climatological maps of physical and biogeochemical tracers
19 to create a surface-to-seafloor, 1° resolution map of nitrate δ^{15}N using an Ensemble of
20 Artificial Neural Networks (EANN). The strong correlation (R_2 > 0.87) and small mean
21 difference (<0.05‰) between EANN-estimated and observed nitrate δ^{15}N indicates that
22 the EANN provides a good estimate of climatological nitrate δ^{15}N without a significant bias.
23 The magnitude of observation-model residuals is consistent with the magnitude of
24 seasonal-decadal changes in observed nitrate δ^{15}N that are not captured by our
25 climatological model. As such, these observation-constrained results provide a globally-
26 resolved map of mean nitrate δ^{15}N for observational and modeling studies of marine
27 biogeochemistry, paleoceanography, and marine ecology.
28
29 **1 Introduction**
30 In contrast to other marine nutrients (e.g., phosphate and silicate), the inventory of nitrate
31 (NO_3^-) is mediated by biological processes, where the main source is N_2 fixation by
32 diazotrophic phytoplankton and the main sink is denitrification (via a microbial
33 consortium in oxygen deficient waters and sediments) (Codispoti and Christensen, 1985).
34 Biological processes also determine the distribution of marine nitrate throughout the water
35 column, with phytoplankton assimilating nitrate / lowering nitrate concentrations in the
36 surface ocean and the microbially-mediated degradation of organic matter in the
37 subsurface. (The latter involving the multi-step process of ammonification (organic matter
38 → NH_4^+) and nitrification (NH_4^+ → NO_2^- → NO_3^-).) By regulating the global inventory and
39 distribution of marine nitrate, these N cycling processes control global net primary
40 productivity, the transfer of nutrients to higher trophic levels such as fishes, and the
41 strength of the ocean's biological carbon pump (Dugdale and Goering, 1967).
42
43 Each of these biologically mediated N transformations affects the N isotopic composition of
44 nitrate in unique ways (Fig.s 1A & 1B and see Section 2), adjusting the relative abundance
45 of ^{15}N and ^{14}N in oceanic nitrate relative to the atmosphere. δ^{15}N = (^{15}N/^{14}Nsample /

46   $^{15}N/^{14}N$standard) – 1), multiplied by 1000 to give units of per mil (‰); see (Sigman and
47   Casciotti, 2001) for simplified equations from (Mariotti et al., 1981). Nitrate $\delta^{15}N$
48   measurements have become a powerful tool for understanding the 'biogeochemical history'
49   of marine nitrate, which includes nitrate assimilation by phytoplankton (Miyake and Wada,
50   1967; Wada and Hattori, 1978), nitrogen fixation (Carpenter et al., 1997; Hoering & Ford,
51   1960), denitrification (Liu, 1979), and nitrification (Casciotti et al., 2013). For example, the
52   consumption of nitrate by denitrification (red line in Fig. 1A) has a larger impact on the
53   residual nitrate $\delta^{15}N$ than does partial nitrate assimilation by phytoplankton (yellow line in
54   Fig. 1), and thus very high $\delta^{15}N$ values serve as a fingerprint of denitrification. Nitrate $\delta^{15}N$
55   is also influenced by the addition of nitrate via remineralization of organic matter. The
56   exact influence of remineralization depends on the isotopic composition of the organic
57   matter, and could result in both higher or lower nitrate $\delta^{15}N$ (Fig. 1A). Nitrate introduced
58   into the water column by the remineralization of organic matter formed by N_2-fixing
59   phytoplankton has an isotopic composition close to that of air (0-1%), and serves to lower
60   the mean ocean $\delta^{15}N$ (Fig. 1B). On the other hand, organic matter formed in regions where
61   the plankton use of most of the available nitrate can be isotopically heavy, and its
62   remineralization will increase the $\delta^{15}N$ of ambient nitrate (Fig. 1B). The actual value of
63   organic matter $\delta^{15}N$ is determined by: (1) the $\delta^{15}N$ of nitrate delivered to the euphotic zone
64   (the subsurface source), which in turn is dependent on the degree of water-column
65   denitrification and (2) the degree of nitrate consumption at the ocean surface, with heavier
66   values associated with greater nitrate consumption (Fig. 1B). Accordingly, changes in
67   organic matter $\delta^{15}N$ (and therefore sediment $\delta^{15}N$ used for paleoceanographic work) can
68   reflect variability of the source nitrate $\delta^{15}N$ and/or variability of the degree of nitrate
69   consumption (e.g., see (Rafter and Charles, 2012)).
70
71   Because of nitrate's place at the base of the marine ecosystem, nitrate $\delta^{15}N$ is also useful for
72   understanding the lifecycles of higher trophic level organisms such as fish (Graham et al.,
73   2007; Tawa et al., 2017) and fishery productivity (Finney et al., 2002, 2000). The $\delta^{15}N$ of
74   whole sediment and microfossils provides insight *by proxy* of past ocean nitrate
75   transformations (Altabet and Francois, 1994; Galbraith et al., 2008; Kienast et al., 2008;
76   Rafter et al., 2012; Robinson et al., 2004; Sigman et al., 1999b)—work that places important
77   constraints on modern ocean N cycling (Altabet, 2007; Eugster et al., 2013; Ren et al.,
78   2017). With an understanding of the N transformations described above and their
79   influences on the N isotopic composition of nitrate, we can begin using nitrate $\delta^{15}N$
80   measurements to trace the integrated biogeochemical history of marine nitrate. However,
81   identifying basin- and global-scale trends in nitrate $\delta^{15}N$ is challenged by the limited spatial
82   extent of nitrate $\delta^{15}N$ observations (Fig. 2). Here, we compile a global database of nitrate
83   $\delta^{15}N$ measurements (Fig. 2) and use an Ensemble Artificial Neural Network (EANN) to
84   produce a map of the global nitrate $\delta^{15}N$ distribution at 1-degree spatial resolution. We find
85   that the mapped nitrate $\delta^{15}N$ climatology matches the observations well and should be a
86   valuable tool for estimating mean conditions and for constraining predictive nitrate $\delta^{15}N$
87   models (Somes et al., 2010; Yang and Gruber, 2016). Below we briefly discuss how the
88   EANN was used to produce global maps of nitrate $\delta^{15}N$ (Section 2), address the ability of
89   the EANN to match the measured $\delta^{15}N$ (Section 3), and examine the EANN-mapped $\delta^{15}N$

90   climatology and global compilation of nitrate $\delta^{15}N$ in the context of published work
91   (Section 4).
92
93   **2 Methods**
94   **2.1 Data Compilation**
95   Nitrate $\delta^{15}N$ observations (Fig. 2; references in Table 3) were compiled from studies dating
96   from 1975 (Cline and Kaplan, 1975) to 2018 (Fripiat et al., 2018), including data from the
97   GEOTRACES Intermediate Data Product (Schlitzer et al., 2018). Whenever possible, the
98   data was acquired via the original author, but in other cases the data was estimated from
99   the publication directly. All observations were treated equally, although the failure to
100   remove nitrite when using the "denitrifier method" may bias the nitrate $\delta^{15}N$ to low values
101   (Rafter et al., 2013). These measurements have been identified as "nitrate+nitrite" in the
102   dataset to acknowledge this potential biasing, which predominantly affects observations in
103   the upper 100 m (Kemeny et al., 2016; Rafter et al., 2013).
104
105   **2.2 Building the neural network model**
106   We utilize an ensemble of artificial neural networks (EANNs) to interpolate our global
107   ocean nitrate $\delta^{15}N$ database (Fig. 2), producing complete 3D maps of the data. By utilizing
108   an artificial neural network (ANN), a machine learning approach that effectively identifies
109   nonlinear relationships between a target variable (the isotopic dataset) and a set of input
110   features (other available ocean datasets), we can fill holes in our data sampling coverage of
111   nitrate $\delta^{15}N$.
112
113   **2.2.1 Binning target variables (Step 1)**
114   We binned the nitrate $\delta^{15}N$ observations (red symbols in Fig. 2) to the World Ocean Atlas
115   2009 (WOA09) grid with a 1-degree spatial resolution and 33 vertical depth layers (0-5500
116   m) (Garcia et al., 2010). When binning vertically, we use the midpoint between the depth
117   values of one layer and the next as the partition between bins (e.g. the first depth layer has
118   a value of 0 m, the second of 10 m, and the third of 20 m, so all nitrate isotopic data
119   sampled between 0-5 m fall in the 0 m bin; between 5-15 m they fall in the 10 m bin, etc.). A
120   point that lies right at the midpoint between depth intervals is binned to the shallower
121   interval. If more than one raw data point falls in a grid cell we take the average of all those
122   points as the value for that grid cell. Certain whole ship tracks of nitrate $\delta^{15}N$ data were
123   withheld from binning to be used as an independent validation set (see section 2.2.4).
124
125   **2.2.2 Obtaining input features (Step 2)**
126   Our input dataset contains a set of climatological values for physical and biogeochemical
127   ocean parameters that form a non-linear relationship with the target data. These include
128   objectively analyzed annual-mean fields for temperature, salinity, nitrate, oxygen, and
129   phosphate taken from the WOA09
130   (https://www.nodc.noaa.gov/OC5/WOA09/woa09data.html) at 1-degree resolution.
131   Additionally, daily chlorophyll data from Modis Aqua for the period Jan-1-2003 through
132   Dec-31-2012 is binned to the WOA09 grid (as described in Step 1) to produce a
133   climatological field of chlorophyll values, which we then log transform to reduce their
134   dynamic range.

Biogeosciences
Discussions

135
2.2.3 Training the ANN (Step 3)
136
137   The architecture of our ANN consists of a single hidden layer, containing 25 nodes, that
138   connects the biological and physical input features (discussed in Step 2) to the target
139   nitrate isotopic variable (as discussed in Step 1). The number of nodes in this hidden layer,
140   as well as the number of input features, determines the number of adjustable weights (the
141   free parameters) in the network. Because there is a danger of over-fitting the model, which
142   occurs when the ANN is over-trained on a dataset so that it cannot generalize well when
143   presented with new data, it is a good practice to have a large number of training data
144   ($\approx$7000 binned data points) relative to the number of weights (200 free parameters). A
145   nonlinear activation function transforms the product of the weights and input features,
146   creating the values assigned to nodes in the hidden layer. Our model utilizes the hyperbolic
147   tangent as its activation function between the input and hidden layer as well as between
148   the hidden and output layer due to its relative speed and general performance (Thimm and
149   Fiesler, 1997). At the output layer, the network produces a prediction of the target nitrate
150   isotopic data (t_{pred}), which it then compares to the actual values of that dataset (t_{data}). The
151   ANN attempts to minimize the value of the cost function
152

$$\text{cost} = \frac{\sum_{i=1}^{n}(t_{pred}^{i} - t_{data}^{i})^2}{n}$$

153
154   by iteratively adjusting the weights using the Levenberg-Marquardt algorithm (Marquardt,
155   1963).
156
2.2.4 Validating the ANN (Step 4)
157
158   To ensure good generalization of the trained ANN to novel data, we randomly withhold
159   10% of the target isotopic data (t_{data}) to be used as an internal validation set for each
160   network. This is data that the network never sees, meaning it does not factor into the cost
161   function, so it works as a test of the ANN's ability to generalize. This internal validation set
162   acts as a gate-keeper to prevent poor models from being accepted into the ensemble of
163   trained networks. Our pass criterion is an R^2 value greater than 0.9 between the ANN's
164   predicted value and the actual values of the validation set. A second, independent or
165   'external' validation set (blue symbols in Fig. 2), composed of complete ship transects from
166   the high and low latitude ocean were omitted from binning in Step 1 and used to establish
167   the performance of the entire ensemble. This independent validation set is never used in
168   the process of developing our ensemble of ANNs.
169
2.2.5 Forming the Ensemble (Step 5)
170
171   The ensemble is formed by repeating Steps 3 to 4 until we obtain 25 trained networks for
172   the nitrate $\delta^{15}N$ dataset. Using an EANN instead of any single network provides several
173   advantages. For example, the random initialization of the weight values in each network as
174   well as differences in the training and internal validation sets used across members make it
175   possible for many different networks to achieve similar performance on their respective
176   validation set while generalizing areas with no data coverage differently. By performing
177   this type of data subsampling and taking an ensemble average, similar to bootstrap

Biogeosciences
Discussions

Open Access
EGU

178   aggregating (Breiman, 1996) this approach improves the robustness of the generalization

179   in areas without data coverage, as demonstrated by the improved performance of the

180   ensemble versus any single member on the independent validation set. The range of values

181   given by the ensemble also provides a measure of the uncertainty for our estimations of

182   δ^{15}N.

183

184   **3 Results**

185   **3.1 Global nitrate δ^{15}N observations**

186   The global compilation of nitrate δ^{15}N includes 1180 stations from all major ocean basins

187   and some minor seas (Fig. 2) giving a total of 12277 nitrate δ^{15}N measurements. Within

188   this dataset, 1197 nitrate δ^{15}N measurements were withheld from the EANN and used to

189   validate the EANN results to ensure good extrapolation (the 'external' validation dataset;

190   blue symbols in Fig. 2, see Section 2). With observations from the surface to as deep as

191   6002 m (Rafter et al., 2012), we find that nitrate δ^{15}N ranges from ≈1‰ in the North

192   Atlantic (e.g., Marconi et al., 2015) to 68.7‰ in the Eastern Tropical South Pacific

193   (Bourbonnais et al., 2015). Nitrate δ^{15}N of ≈1‰ was also irregularly observed in the

194   shallow North and South Pacific (Liu et al., 1996; Yoshikawa et al., 2015). These latter

195   observations were included in the training dataset, although we should note that the

196   measurements using the 'Devarda's Alloy' method (Liu et al., 1996) is thought to be biased

197   low (Altabet and Francois, 2001). Similarly, the inclusion of nitrite for 'denitrifier method'

198   nitrate δ^{15}N can bias the measurement to lower values (Kemeny et al., 2016; Rafter et al.,

199   2013).

200

201   **3.2 Marine nitrate δ^{15}N observations-model comparison**

202   The observed and EANN-predicted nitrate δ^{15}N measurements are distributed around a 1:1

203   line in Fig. 3A (all data), with considerably less scatter for the deeper values (data >1000 m;

204   Fig. 3B). The correlation coefficient of determination for the observations versus the model

205   nitrate δ^{15}N gives an R^2=0.75 for the observations used to train the EANN and an R^2 of 0.78

206   for the validation dataset. We can also examine the performance of the EANN with the

207   nitrate δ^{15}N "residual" or the difference between observed and modeled δ^{15}N, which

208   indicates a mean residual or 'mean bias' value of -0.03‰ for the entire dataset and

209   +0.18‰ for the validation dataset.

210

211   Examining the observation-EANN residuals via the Root Mean Square Error (RMSE), we

212   find an RMSE of 1.94‰ for the data used to train the EANN and an RMSE of 1.26‰ for the

213   external validation dataset. There is a clear relationship between RMSE and depth, with a

214   significantly higher RMSE for the upper 500 m (Figs. 3C and 3D). Comparing these residual

215   values with dissolved oxygen concentrations (color in Fig. 3C), we find that >2‰ RMSE for

216   the surface is associated with high oxygen while >2.7‰ RMSE at ≈250 m is associated with

217   the lowest oxygen. Furthermore, the RMSE of the observation-EANN residuals differs

218   between the datasets used to train the model (solid red line in Fig. 3D) and validate the

219   model (dashed line in Fig. 3D).

220

221   The RMSE patterns in Figs. 3C and 3D are to be expected given the natural variability in

222   nitrate δ^{15}N driven by assimilation in the upper ocean and denitrification in the shallow

Biogeosciences
Discussions

223   sub-surface—variability which is not captured by the climatological EANN. Rafter and
224   Sigman (2016), presented a 5-year time-series of nitrate δ^{15}N from the eastern equatorial
225   Pacific, which showed that variability of nitrate assimilation produces seasonal-to-
226   interannual deviations of δ^{15}N of ±2.5‰, which is similar to the magnitude of the RMSE in
227   the surface ocean (2.2‰). Although there are no nitrate δ^{15}N time-series measurements
228   from the subsurface Oxygen Deficient Zone (ODZ) waters where denitrification occurs,
229   nitrate δ^{15}N in ODZs presumably have similar seasonal-to-interannual (or longer timescale)
230   variability due to changes in the rate and extent of water column denitrification (Deutsch et
231   al., 2011; Yang et al., 2017). For example, a larger degree of nitrate undergoing water
232   column denitrification would explain the extreme δ^{15}N values at the bottom right of Fig.
233   3A—observations that all come from the ODZ waters of the Eastern Tropical South Pacific
234   (Bourbonnais et al., 2015; Casciotti et al., 2013; Rafter et al., 2012; Ryabenko et al., 2012).
235   Some of these very high nitrate δ^{15}N values are associated with nitrate concentrations <1
236   µmol kg^{-1} (Bourbonnais et al., 2015), values much lower than within our climatology for
237   the subsurface Eastern Tropical South Pacific. These values thus represent episodic
238   denitrification events that the EANN will not be able to capture because it is trained on
239   climatological data. In the deep ocean where temporal variability is negligible, the
240   observation-EANN residuals of 0.2‰ are the same magnitude as the δ^{15}N analytical errors,
241   further emphasizing the ability of the model to match climatological average conditions.
242
243   **4 Discussion**
244   The EANN's skillful estimate of mean marine nitrate δ^{15}N can be useful for all areas of
245   research using this widely used geochemical measurement. The zonal average view of
246   EANN nitrate δ^{15}N for each major ocean basin (Fig. 4) includes statistics comparing the
247   observations versus EANN results above and below 1000 m. These region-specific statistics
248   indicated a weaker correlation between EANN and observed nitrate δ^{15}N in the deep
249   Atlantic and Southern Ocean, despite low RMSE and negligible mean bias. This weak
250   correlation likely derives from the limited range of deep nitrate δ^{15}N variability (±0.1‰) in
251   these basins (see Fig. 5D).
252
253   The nitrate δ^{15}N sections in Fig. 4 also show elevated values for the low latitude, upper
254   mesopelagic Pacific (Fig. 4A) and Indian Oceans (Fig. 4D) where water column
255   denitrification raises the residual nitrate δ^{15}N (Fig. 1A). Viewing this elevated nitrate δ^{15}N
256   at the 250 m depth horizon (Fig. 5) better reveals the spatial heterogeneity of the
257   observations and EANN results. (It is because of this intra-basin heterogeneity, and the fact
258   that many observations are biased towards the areas of denitrification, that we did not plot
259   the observed nitrate δ^{15}N within the zonally-averaged Fig. 4 views.) The EANN error for the
260   Fig. 5 depth intervals (Figs. 5E-5H) is the standard deviation of the 25 ensemble members
261   of the EANN and shows a decrease in ensemble variability with depth—a trend that is
262   consistent with the overall decrease in observed nitrate δ^{15}N variability with depth (Figs. 4
263   & 5).
264
265   Below we inspect the observed and EANN-predicted nitrate δ^{15}N and discuss the
266   consistency of these results with our understanding of published work. This analysis begins
267   with the spatial distribution of nitrate delivered to the upper ocean. We then discuss the

Biogeosciences
Discussions

EGU
Open Access

268   impacts of upper ocean nitrate assimilation on organic matter $\delta^{15}N$ and consider the
269   influence of organic matter remineralization on sub-surface nitrate.
270
271   **4.1 Subsurface and surface nitrate $\delta^{15}N$**
272   The nitrate $\delta^{15}N$ distribution at 250 m depth (Fig. 5B) offers a view of nitrate at a depth
273   that is deeper than source waters in many ocean regions (e.g., 100 to 150 m in the
274   equatorial Pacific (Rafter and Sigman, 2016)), but is negligibly influenced by nitrate
275   assimilation, and therefore provides a qualitative view of spatial trends in nitrate delivered
276   to the surface ocean. Nitrate $\delta^{15}N$ at this depth is highest in the North and South Eastern
277   Tropical Pacific and Arabian Seas (Fig. 5B), due to the influence of water column
278   denitrification in the ODZs in these regions (Altabet et al., 2012; Bourbonnais et al., 2015;
279   Ryabenko et al., 2012), which preferentially uses the light isotope and leaves the residual
280   nitrate enriched in ^{15}N.
281
282   Lowest $\delta^{15}N$ values of sub-surface nitrate are found in the Southern Ocean and in the North
283   Atlantic. The North Atlantic subtropical gyre in particular has the lowest $\delta^{15}N$ values in any
284   basin (Fig. 5B; also see (Fawcett et al., 2011; Knapp et al., 2005, 2008)), which can be
285   attributed to the remineralization of low-$\delta^{15}N$ organic matter originating from N_2-fixation,
286   which has a $\delta^{15}N$ between 0 and -1‰ (similar to atmospheric N_2; see Fig. 1B (Carpenter et
287   al., 1997; Hoering & Ford, 1960)). Prior work argues that this nitrate $\delta^{15}N$ lowering
288   requires the bulk of Atlantic N_2-fixation (≈90%) to occur in the tropics (Marconi et al.,
289   2017) followed by the advection of remineralized nitrate to the North Atlantic. This
290   contrasts with numerical models arguing for high N_2-fixation rates in the North Atlantic
291   (Ko et al., 2018). Similar local minima of sub-surface $\delta^{15}N$ appear in all the sub-tropical
292   gyres (Fig. 5B), which is consistent with observations (Casciotti et al., 2008; Yoshikawa et
293   al., 2015) and presumably indicates the importance of N_2-fixation in these regions (Ko et
294   al., (2018) and others). The N_2-fixation $\delta^{15}N$ signal in the Pacific Ocean is counteracted by
295   the influence of water-column denitrification in that basin, which imparts a high $\delta^{15}N$
296   signal, but a local minimum in $\delta^{15}N$ can still be seen in the Pacific subtropical gyres (Fig.
297   4A).
298
299   Nitrate assimilation by phytoplankton in the upper ocean is influenced by both the
300   subsurface source nitrate $\delta^{15}N$ and the degree of nitrate assimilation (Miyake and Wada,
301   1967; Wada and Hattori, 1978) (Fig. 1B). This gives the expectation that average nitrate
302   $\delta^{15}N$ values for the upper 50 m (Fig. 5A) will be consistently higher than those at 250 m
303   (Fig. 5B). However, the highest values in the upper 50 m are not found above the ODZ
304   regions, but are on the edges of high nitrate concentration upwelling zones in the Southern
305   Ocean, equatorial Pacific, and subarctic gyres (contours in Fig. 2). Circulation in these 'edge'
306   regions allows for nitrate to be advected along the surface, lengthening its time in the
307   surface ocean and allowing more utilization to elevate the residual nitrate $\delta^{15}N$ pool. In
308   other words, the degree of nitrate utilization appears to play a more important role in
309   determining surface nitrate $\delta^{15}N$ than the initial value. (This is not the case for the organic
310   matter $\delta^{15}N$ produced from this nitrate, which will be discussed more below and in Fig. 1B.)
311

312   Despite our expectation of higher nitrate $\delta^{15}N$ in the upper 50 m versus 250 m (Figs. 5A vs.
313   5B), we identify two types of regions where this difference is negative (Fig. 6): above ODZ
314   waters and in subtropical gyres. The explanation for the negative values above the ODZ
315   regions is that the nitrate $\delta^{15}N$ at 250 m must be much higher than the nitrate $\delta^{15}N$
316   upwelled to the surface. This is consistent with elevated ODZ nitrate $\delta^{15}N$ having an
317   indirect path to waters outside of ODZ regions (Peters et al., 2017; Rafter et al., 2013). The
318   subtropical gyres also have modeled nitrate $\delta^{15}N$ in the upper 50 m that is less than 250 m,
319   but this finding is difficult to test with observations because of low nitrate concentrations.
320   That said, the model predicts a lowering of the nitrate $\delta^{15}N$ in the upper ocean relative to
321   the 250 m depths, which is consistent with N_2-fixation in these regions.
322
323   Our discussion above highlights the difficulty of distinguishing between the competing
324   influences of the subsurface source nitrate $\delta^{15}N$ and the degree of nitrate utilization on
325   residual nitrate $\delta^{15}N$. Clearly a static depth does not reflect the subsurface source of nitrate
326   delivered to the surface and a more robust method for estimating this subsurface source
327   needs to be developed. However, some generalizations can be made regarding the organic
328   matter $\delta^{15}N$ produced in these regions and its potential influence (via remineralization) on
329   subsurface nitrate throughout the water column via the export and remineralization of
330   organic matter (Sigman et al., 2009). For example, a local minimum in $\delta^{15}N$ is visible at 250
331   m depth in the Eastern Equatorial Pacific (Fig. 5B; also discussed in several studies (Rafter
332   et al., 2012; Rafter and Sigman, 2016)) is caused by the remineralization of organic matter
333   with a low $\delta^{15}N$ due to partial nitrate consumption at the surface. Below we discuss these
334   and other influences on intermediate-depth nitrate $\delta^{15}N$.
335
336   **4.2 Intermediate-depth nitrate $\delta^{15}N$ variability**
337   Waters at "intermediate" depths (here shown as the 750 m surface in Fig. 5C) are important
338   because they are part of a large-scale circulation that initially upwells in the Southern
339   Ocean and ultimately resupplies nutrients to the low latitude thermocline (Palter et al.,
340   2010; Sarmiento et al., 2004; Toggweiler et al., 1991; Toggweiler and Carson, 1995). Within
341   the context of this overturning, the nitrate upwelling in the Southern Ocean is initially
342   ≈5‰ (Figs. 4C & 5C) and the $\delta^{15}N$ is elevated ≈2‰ by partial nitrate assimilation in
343   surface waters as they are advected equatorward (see Figs. 5A and 6). Deep winter-time
344   mixing in the Subantarctic Pacific converts these surface waters into mode and
345   intermediate waters (Herraiz-Borreguero and Rintoul, 2011), introducing nitrate with a
346   "pre-formed" $\delta^{15}N$ of ≈6‰ into the intermediate-depth South Pacific and South Atlantic
347   (Rafter et al., 2012, 2013; Tuerena et al., 2015) at depths between ≈600-1200 m. The
348   penetration of this pre-formed signal (nitrate ≥ 6‰) into the interior can be clearly seen in
349   the Atlantic Ocean between ≈40°S to 20°N (Fig. 4B).
350
351   The same signal is carried with Southern Ocean mode and intermediate waters into the
352   Pacific basin (Rafter et al., 2013), although it is difficult to distinguish in the model results
353   against the higher background $\delta^{15}N$ in this basins (Figs. 4A, 4D, 5C). The same process
354   presumably introduces elevated nitrate $\delta^{15}N$ to the Indian Ocean, which has similar values
355   at this depth. Nitrate $\delta^{15}N$ increases from the Southern Ocean toward the equator in the
356   Pacific and Indian Oceans, but not in the Atlantic (Fig. 5C). Organic matter has a lower $\delta^{15}N$

357   in the Atlantic than in the Pacific and Indian because of a lack of water-column
358   denitrification supplying high-δ^{15}N water to the surface, and because of the high rates of
359   N$_2$-fixation which supply isotopically light N to organic matter (Marconi et al., 2017;
360   Tuerena et al., 2015). This contrast in intermediate-depth nitrate δ^{15}N can be traced to the
361   lower δ^{15}N of organic matter remineralized in this region—an explanation that is also
362   consistent with enhanced N$_2$ fixation in the tropical Atlantic (Marconi et al., 2017). The
363   increase in intermediate-depth nitrate δ^{15}N from the Subantarctic to the tropical Pacific
364   appears to result from the remineralization of organic matter with a δ^{15}N elevated by high
365   source nitrate δ^{15}N (near the ODZ) or extreme elevation of residual nitrate δ^{15}N (advected
366   along the surface away from the equator; see high surface nitrate δ^{15}N in Fig. 5A). Previous
367   work suggests that direct mixing with denitrified waters represents only a small fraction of
368   the change from the pre-formed high latitude value (≈6‰) to tropical nitrate δ^{15}N of ≈7‰
369   (Peters et al., 2017; Rafter et al., 2013; Rafter and Charles, 2012). Equivalent processes
370   must drive the δ^{15}N in the intermediate-depth Indian Ocean, which is similarly elevated in
371   the EANN, although direct observations are needed in order to confirm how well the EANN
372   extrapolates in this region.
373
374   **4.4 Deep-sea nitrate δ^{15}N trends**
375   Our discussion above suggests that the basin-scale balance of N$_2$-fixation and water-column
376   denitrification is a major contributor to inter-basin nitrate δ^{15}N gradients in the upper
377   ocean, lowering values in the Atlantic Oceans compared to the Pacific and Indian Oceans.
378   Averaging EANN nitrate δ^{15}N from the surface to 5500 m for each ocean basin (Fig. 7), we
379   find that these basin-scale nitrate δ^{15}N differences also persist into the deep-sea. (Note that
380   the basin-scale model nitrate δ^{15}N differences shown in Fig. 7 are even larger for the nitrate
381   δ^{15}N observations because the measurements are spatially biased towards areas of water
382   column denitrification in the Pacific and Indian Oceans (see Fig. 2).)
383
384   The remineralization of organic matter is one process that can—and has been used to—
385   explain both the elevation of deep Pacific nitrate δ^{15}N (Peters et al., 2017; Rafter et al.,
386   2013; Sigman et al., 2009) and lowering of deep Atlantic nitrate δ^{15}N (Knapp et al., 2008;
387   Marconi, 2017; Marconi et al., 2017; Tuerena et al., 2015) relative to the deep ocean mean.
388   Here we provide two additional pieces of evidence that argue for the remineralization of
389   organic matter as the key driver of these deep-sea nitrate δ^{15}N differences. Our first piece
390   of evidence is that the average subsurface source of nitrate to the Pacific and Indian Ocean
391   surface has a significantly higher δ^{15}N (by 2‰ at the 250 m depth surface) than the
392   Atlantic and Southern Oceans (Figs. 5B and 7). Nitrate δ^{15}N at 250 m is an admittedly
393   imprecise estimate for the nitrate upwelled to the surface, but even a slight elevation in
394   Pacific source nitrate δ^{15}N and near complete nitrate utilization at the surface will translate
395   into higher sinking organic matter δ^{15}N (i.e., see Fig. 1B).
396
397   Our second piece of evidence that the export and remineralization of organic matter drives
398   the inter-basin differences in deep nitrate δ^{15}N comes from sediment trap measurements.
399   Averaging published sediment trap organic matter δ^{15}N from the subtropical and tropical
400   Pacific gives a value of 8.5±2.9‰ (Knapp et al., 2016; Robinson et al., 2012), which is

401　significantly higher than measured in traps from the Atlantic (4.5±1.5‰) (Freudenthal et
402　al., 2001; Holmes et al., 2002; Lavik, 2000; Thunell et al., 2004). Given observed Southern
403　Ocean nitrate characteristics (Rafter et al., 2013), we estimate an even lower typical sinking
404　organic matter δ^{15}N of +1.5‰ for this region. (This assumes initial values are the Upper
405　Circumpolar Deep Water and final values from the Open Antarctic Zone. Published results
406　from the iron-fertilized Kerguelen Plateau region are predictably higher (Trull et al.,
407　2008).) The much lower Southern Ocean sinking organic matter δ^{15}N is consistent with
408　partial consumption of nitrate at the surface (see Fig. 1B) and the entrainment of this
409　nitrate in equatorward-moving intermediate waters acts to export nitrate with elevated
410　δ^{15}N to intermediate waters throughout the Southern Hemisphere (see discussion above).
411　Based on this evidence, it appears that global patterns of sinking organic matter δ^{15}N are
412　consistent with the remineralization of this organic matter driving subtle, but significant
413　differences in deep-sea nitrate δ^{15}N.
414
415　An alternative explanation for the deep-sea nitrate δ^{15}N differences in Fig. 7 is that they
416　reflect the lateral (along isopycnal) advection of elevated nitrate δ^{15}N from ODZ regions.
417　However, we can easily dismiss this explanation by looking at the meridional trends in
418　deep-sea nitrate δ^{15}N—following the deep waters from their entrance in the south and
419　movement northward. What we find is that deep EANN nitrate δ^{15}N (numbers in Fig. 5D) is
420　lowest in the Southern Ocean and increases equatorward in the Pacific. Average observed
421　nitrate δ^{15}N below 2500 m increases from 4.7±0.1‰ in the Pacific sector of the Southern
422　Ocean to 4.9±0.2‰ in the deep South Pacific, 5.4±0.2‰ in the deep tropical Pacific, and
423　5.2±0.2‰ in the deep North Pacific. This contrasts with no significant change in deep
424　Atlantic nitrate δ^{15}N, despite the export of slightly elevated nitrate δ^{15}N into intermediate-
425　depth Atlantic (see above and (Tuerena et al., 2015)) and the introduction of a different
426　deep water mass (North Atlantic Deep Water) in the North Atlantic. The distribution of
427　deep Pacific nitrate δ^{15}N is coherent with elevated organic matter δ^{15}N being produced and
428　exported from the lower latitude surface and remineralized at depth. In other words, inter-
429　basin differences sinking organic matter δ^{15}N best explains the inter-basin differences in
430　deep EANN and observed nitrate δ^{15}N. Vertical, diapycnal mixing from the low latitude
431　Pacific ODZ regions may also play a role in the south-to-north elevation of deep Pacific
432　nitrate δ^{15}N, but we cannot quantify the magnitude of that influence without a circulation
433　model. Future work should look into this issue.
434
435　**5 Conclusions**
436　We find that an Ensemble of Artificial Neural Networks (EANN) can be trained on
437　climatological distributions of physical and biogeochemical tracers to reproduce a global
438　database of nitrate δ^{15}N observations (Fig. 2) with good fidelity (Fig. 3). We used the EANN
439　to produce global climatological maps of nitrate δ^{15}N at a 1 degree-resolution from the
440　surface to the seafloor. These results help identify spatial patterns (Figs. 4-6) and quantify
441　regional and basin-average oceanic values of nitrate δ^{15}N (Fig. 7). Major differences
442　between the observed and EANN-predicted nitrate δ^{15}N appear to be caused by temporal
443　variability of nitrate δ^{15}N in the upper ocean and in ODZs associated with variable nitrate
444　uptake and denitrification rates. Additional measurements of nitrate δ^{15}N will help to

445   develop seasonally-resolved maps that can improve upon the climatological mean map
446   provided here.
447
453

References

Altabet, M. A.: Constraints on oceanic N balance/imbalance from sedimentary N-15 records, Biogeosciences, 4(1), 75–86, 2007.

Altabet, M. A. and Francois, R.: Sedimentary nitrogen isotopic ratio as a recorder for surface ocean nitrate utilization, Glob. Biogeochem. Cycles, 8(1), 103–116, 1994.

Altabet, M. A. and Francois, R.: Nitrogen isotope biogeochemistry of the antarctic polar frontal zone at 170 degrees W, Deep-Sea Res. Part Ii-Top. Stud. Oceanogr., 48(19–20), 4247–4273, 2001.

Altabet, M. A., Ryabenko, E., Stramma, L., Wallace, D. W. R., Frank, M., Grasse, P. and Lavik, G.: An eddy-stimulated hotspot for fixed nitrogen-loss from the Peru oxygen minimum zone, Biogeosciences, 9(12), 4897–4908, doi:10.5194/bg-9-4897-2012, 2012.

Bourbonnais, A., Altabet, M. A., Charoenpong, C. N., Larkum, J., Hu, H., Bange, H. W. and Stramma, L.: N-loss isotope effects in the Peru oxygen minimum zone studied using a mesoscale eddy as a natural tracer experiment, Glob. Biogeochem. Cycles, 29(6), 793–811, doi:10.1002/2014GB005001, 2015.

Breiman, L.: Bagging predictors, Mach. Learn., 24(2), 123–140, doi:10.1007/BF00058655, 1996.

Carpenter, E. J., Harvey, H. R., Fry, B. and Capone, D. G.: Biogeochemical tracers of the marine cyanobacterium Trichodesmium, Deep-Sea Res. Part -Oceanogr. Res. Pap., 44(1), 27–38, doi:10.1016/s0967-0637(96)00091-x, 1997.

Casciotti, K. L., Trull, T. W., Glover, D. M. and Davies, D.: Constraints on nitrogen cycling at the subtropical North Pacific Station ALOHA from isotopic measurements of nitrate and particulate nitrogen, Deep-Sea Res. Part Ii-Top. Stud. Oceanogr., 55(14–15), 1661–1672, doi:10.1016/j.dsr2.2008.04.017, 2008.

Casciotti, K. L., Buchwald, C. and McIlvin, M.: Implications of nitrate and nitrite isotopic measurements for the mechanisms of nitrogen cycling in the Peru oxygen deficient zone, Deep Sea Res. Part Oceanogr. Res. Pap., 80, 78–93, doi:10.1016/j.dsr.2013.05.017, 2013.

Cline, J. D. and Kaplan, I. R.: Isotopic fractionation of dissolved nitrate during denitrification in the eastern tropical North Pacific Ocean, Mar. Chem., 3(4), 271–299, doi:10.1016/0304-4203(75)90009-2, 1975.

Codispoti, L. . and Christensen, J. .: Nitrification, denitrification and nitrous oxide cycling in the eastern tropical South Pacific ocean, Mar. Chem., 16(4), 277–300, doi:10.1016/0304-4203(85)90051-9, 1985.

Deutsch, C., Brix, H., Ito, T., Frenzel, H. and Thompson, L.: Climate-Forced Variability of Ocean Hypoxia, Science, 333(6040), 336–339, doi:10.1126/science.1202422, 2011.

489   Dugdale, R. C. and Goering, J. J.: Uptake of new and regenerated forms of nitrogen in
490   primary production, Limnol. Oceanogr., 12(2), 196–206, 1967.

491   Eugster, O., Gruber, N., Deutsch, C., Jaccard, S. L. and Payne, M. R.: The dynamics of the
492   marine nitrogen cycle across the last deglaciation, Paleoceanography, 28(1), 116–129,
493   doi:10.1002/palo.20020, 2013.

494   Fawcett, S. E., Lomas, M., Casey, J. R., Ward, B. B. and Sigman, D. M.: Assimilation of upwelled
495   nitrate by small eukaryotes in the Sargasso Sea, Nat. Geosci., 4(10), 717–722,
496   doi:10.1038/ngeo1265, 2011.

497   Finney, B. P., Gregory-Eaves, I., Douglas, M. S. V. and Smol, J. P.: Fisheries productivity in the
498   northeastern Pacific Ocean over the past 2,200 years, Nature, 416(6882), 729–733,
499   doi:10.1038/416729a, 2002.

500   Finney, B. P. et al.: Impacts of Climatic Change and Fishing on Pacific Salmon Abundance
501   Over the Past 300 Years, Science, 290, 795-799., 2000.

502   Freudenthal, T., Neuer, S., Meggers, H., Davenport, R. and Wefer, G.: Influence of lateral
503   particle advection and organic matter degradation on sediment accumulation and stable
504   nitrogen isotope ratios along a productivity gradient in the Canary Islands region, Mar.
505   Geol., 17, 2001.

506   Fripiat, F., Declercq, M., Sapart, C. J., Anderson, L. G., Bruechert, V., Deman, F., Fonseca-
507   Batista, D., Humborg, C., Roukaerts, A., Semiletov, I. P. and Dehairs, F.: Influence of the
508   bordering shelves on nutrient distribution in the Arctic halocline inferred from water
509   column nitrate isotopes, Limnol. Oceanogr., IN PRESS, 2018.

510   Galbraith, E. D., Sigman, D. M., Robinson, R. S. and Pedersen, T. F.: Chapter 34 - Nitrogen in
511   Past Marine Environments, in Nitrogen in the Marine Environment (2nd Edition), pp.
512   1497–1535, Academic Press, San Diego. [online] Available from:
513   http://www.sciencedirect.com/science/article/pii/B9780123725226000347, 2008.

514   Garcia, H. E., Locarnini, T. P., Boyer, T. P., Antonov, J. I., Zweng, M. M., Baranova, O. K. and
515   Johnson, D. R.: Volume 4: Nutrients (phosphate, nitrate, and silicate), in World Ocean Atlas
516   2009, pp. 1–44, U.S. Government Printing Office., 2010.

517   Graham, B. S., Grubbs, D., Holland, K. and Popp, B. N.: A rapid ontogenetic shift in the diet of
518   juvenile yellowfin tuna from Hawaii, Mar. Biol., 150(4), 647–658, doi:10.1007/s00227-006-
519   0360-y, 2007.

520   Herraiz-Borreguero, L. and Rintoul, S. R.: Subantarctic mode water: distribution and
521   circulation, Ocean Dyn., 61(1), 103–126, doi:10.1007/s10236-010-0352-9, 2011.

522   Hoering, T. C. and Ford, H. T.: The isotope effect in the fixation of nitrogen by azotobacter, J.
523   Am. Chem. Soc., 82(2), 376–378, doi:10.1021/ja01487a031, 1960.

524   Holmes, E., Lavik, G., Fischer, G., Segl, M., Ruhland, G. and Wefer, G.: Seasonal variability of
525   d15N in sinking particles in the Benguela upwelling region, , 18, 2002.

526   Kemeny, P. C., Weigand, M. A., Zhang, R., Carter, B. R., Karsh, K. L., Fawcett, S. E. and Sigman,
527   D. M.: Enzyme-level interconversion of nitrate and nitrite in the fall mixed layer of the
528   Antarctic Ocean: Antarctic Fall Nitrate Isotopes, Glob. Biogeochem. Cycles, 30(7), 1069–
529   1085, doi:10.1002/2015GB005350, 2016.

530   Kienast, M., Lehmann, M. F., Timmermann, A., Galbraith, E., Bolliet, T., Holboum, A.,
531   Normandeau, C. and Laj, C.: A mid-Holocene transition in the nitrogen dynamics of the
532   western equatorial Pacific: Evidence of a deepening thermocline?, Geophys. Res. Lett.,
533   35(23), doi:10.1029/2008gl035464, 2008.

534   Knapp, A. N., Sigman, D. M. and Lipschultz, F.: N isotopic composition of dissolved organic
535   nitrogen and nitrate at the Bermuda Atlantic time-series study site, Glob. Biogeochem.
536   Cycles, 19(1), doi:10.1029/2004gb002320, 2005.

537   Knapp, A. N., DiFiore, P. J., Deutsch, C., Sigman, D. M. and Lipschultz, F.: Nitrate isotopic
538   composition between Bermuda and Puerto Rico: Implications for N(2) fixation in the
539   Atlantic Ocean, Glob. Biogeochem. Cycles, 22(3), doi:10.1029/2007gb003107, 2008.

540   Knapp, A. N., Casciotti, K. L., Berelson, W. M., Prokopenko, M. G. and Capone, D. G.: Low rates
541   of nitrogen fixation in eastern tropical South Pacific surface waters, Proc. Natl. Acad. Sci.,
542   113(16), 4398–4403, doi:10.1073/pnas.1515641113, 2016.

543   Ko, Y. H., Lee, K., Takahashi, T., Karl, D. M., Kang, S.-H. and Lee, E.: Carbon-Based Estimate of
544   Nitrogen Fixation-Derived Net Community Production in N-Depleted Ocean Gyres, Glob.
545   Biogeochem. Cycles, doi:10.1029/2017GB005634, 2018.

546   Lavik, G.: Nitrogen isotopes of sinking matter and sediments in the South Atlantic,
547   Universität Bremen, Bremen, Deutschland., 2000.

548   Liu, K. K.: Geochemistry of inorganic nitrogen compounds in two marine environments: The
549   Santa Barbara Basin and the ocean off Peru, University of Southern California, Los Angeles.,
550   1979.

551   Liu, K. K., Su, M. J., Hsueh, C. R. and Gong, G. C.: The nitrogen isotopic composition of nitrate
552   in the Kuroshio Water northeast of Taiwan: Evidence for nitrogen fixation as a source of
553   isotopically light nitrate, Mar. Chem., 54(3–4), 273–292, doi:10.1016/0304-
554   4203(96)00034-5, 1996.

555   Marconi, D.: Use of the nitrate isotopes in the ocean interior to explore the isotopic
556   compisition of sinking nitrogen and its implications for marine biogeochemical cycles, ,
557   297, 2017.

558   Marconi, D., Alexandra Weigand, M., Rafter, P. A., McIlvin, M. R., Forbes, M., Casciotti, K. L.
559   and Sigman, D. M.: Nitrate isotope distributions on the US GEOTRACES North Atlantic

560   cross-basin section: Signals of polar nitrate sources and low latitude nitrogen cycling, Mar.
561   Chem., 177, 143–156, doi:10.1016/j.marchem.2015.06.007, 2015.

562   Marconi, D., Sigman, D. M., Casciotti, K. L., Campbell, E. C., Alexandra Weigand, M., Fawcett,
563   S. E., Knapp, A. N., Rafter, P. A., Ward, B. B. and Haug, G. H.: Tropical Dominance of N2
564   Fixation in the North Atlantic Ocean: Tropical Lead of Atlantic N2 fixation, Glob.
565   Biogeochem. Cycles, 31(10), 1608–1623, doi:10.1002/2016GB005613, 2017.

566   Mariotti, A., Germon, J. C., Hubert, P., Kaiser, P., Letolle, R., Tardieux, A. and Tardieux, P.:
567   Experimental determination of nitrogen kinetic isotope fractionation—some principles—
568   illustration for the denitrification and nitrification processes, Plant Soil, 62(3), 413–430,
569   1981.

570   Marquardt, D. W.: An Algorithm for Least-Squares Estimation of Nonlinear Parameters, J.
571   Soc. Ind. Appl. Math., 11(2), 431–441, doi:10.1137/0111030, 1963.

572   Miyake, Y. and Wada, E.: The Abundance Ratio of 15N/14N in Marine Environments, Rec.
573   Oceanogr. Works Jpn., 9(l), 1967.

574   Palter, J. B., Sarmiento, J. L., Gnanadesikan, A., Simeon, J. and Slater, R. D.: Fueling export
575   production: nutrient return pathways from the deep ocean and their dependence on the
576   Meridional Overturning Circulation, Biogeosciences, 7(11), 3549–3568, doi:10.5194/bg-7-
577   3549-2010, 2010.

578   Peters, B. D., Lam, P. J. and Casciotti, K. L.: Nitrogen and oxygen isotope measurements of
579   nitrate along the US GEOTRACES Eastern Pacific Zonal Transect (GP16) yield insights into
580   nitrate supply, remineralization, and water mass transport, Mar. Chem.,
581   doi:10.1016/j.marchem.2017.09.009, 2017.

582   Rafter, P. A. and Charles, C. D.: Pleistocene equatorial Pacific dynamics inferred from the
583   zonal asymmetry in sedimentary nitrogen isotopes, Paleoceanography, 27,
584   doi:10.1029/2012pa002367, 2012.

585   Rafter, P. A. and Sigman, D. M.: Spatial distribution and temporal variation of nitrate
586   nitrogen and oxygen isotopes in the upper equatorial Pacific Ocean, Limnol. Oceanogr.,
587   61(1), 14–31, doi:10.1002/lno.10152, 2016.

588   Rafter, P. A., Sigman, D. M., Charles, C. D., Kaiser, J. and Haug, G. H.: Subsurface tropical
589   Pacific nitrogen isotopic composition of nitrate: Biogeochemical signals and their transport,
590   Glob. Biogeochem. Cycles, 26, doi:10.1029/2010gb003979, 2012.

591   Rafter, P. A., DiFiore, P. J. and Sigman, D. M.: Coupled nitrate nitrogen and oxygen isotopes
592   and organic matter remineralization in the Southern and Pacific Oceans, J. Geophys. Res.
593   Oceans, 118, 1–14, doi:10.1002/jgrc.20316, 2013.

594   Ren, H., Chen, Y.-C., Wang, X. T., Wong, G. T. F., Cohen, A. L., DeCarlo, T. M., Weigand, M. A.,
595   Mii, H.-S. and Sigman, D. M.: 21st-century rise in anthropogenic nitrogen deposition on a
596   remote coral reef, Science, 356(6339), 749–752, doi:10.1126/science.aal3869, 2017.

597   Robinson, R. S., Brunelle, B. G. and Sigman, D. M.: Revisiting nutrient utilization in the glacial
598   Antarctic: Evidence from a new method for diatom-bound N isotopic analysis,
599   Paleoceanography, 19(3), doi:10.1029/2003pa000996, 2004.

600   Robinson, R. S., Kienast, M., Albuquerque, A. L., Altabet, M., Contreras, S., Holz, R. D., Dubois,
601   N., Francois, R., Galbraith, E., Hsu, T. C., Ivanochko, T., Jaccard, S., Kao, S. J., Kiefer, T., Kienast,
602   S., Lehmann, M. F., Martinez, P., McCarthy, M., Mobius, J., Pedersen, T., Quan, T. M.,
603   Ryabenko, E., Schmittner, A., Schneider, R., Schneider-Mor, A., Shigemitsu, M., Sinclair, D.,
604   Somes, C., Studer, A., Thunell, R. and Yang, J. Y.: A review of nitrogen isotopic alteration in
605   marine sediments, Paleoceanography, 27, doi:10.1029/2012pa002321, 2012.

606   Ryabenko, E., Kock, A., Bange, H. W., Altabet, M. A. and Wallace, D. W. R.: Contrasting
607   biogeochemistry of nitrogen in the Atlantic and Pacific Oxygen Minimum Zones,
608   Biogeosciences, 9(1), 203–215, doi:10.5194/bg-9-203-2012, 2012.

609   Sarmiento, J. L., Gruber, N., Brzezinski, M. A. and Dunne, J. P.: High-latitude controls of
610   thermocline nutrients and low latitude biological productivity, Nature, 427(6969), 56–60,
611   doi:10.1038/nature02127, 2004.

612   Schlitzer, R., Anderson, R. F., Dodas, E. M., Lohan, M., Geibert, W., Tagliabue, A., Bowie, A.,
613   Jeandel, C., Maldonado, M. T., Landing, W. M., Cockwell, D., Abadie, C., Abouchami, W.,
614   Achterberg, E. P., Agather, A., Aguliar-Islas, A., van Aken, H. M., Andersen, M., Archer, C.,
615   Auro, M., de Baar, H. J., Baars, O., Baker, A. R., Bakker, K., Basak, C., Baskaran, M., Bates, N. R.,
616   Bauch, D., van Beek, P., Behrens, M. K., Black, E., Bluhm, K., Bopp, L., Bouman, H., Bowman,
617   K., Bown, J., Boyd, P., Boye, M., Boyle, E. A., Branellec, P., Bridgestock, L., Brissebrat, G.,
618   Browning, T., Bruland, K. W., Brumsack, H.-J., Brzezinski, M., Buck, C. S., Buck, K. N.,
619   Buesseler, K., Bull, A., Butler, E., Cai, P., Mor, P. C., Cardinal, D., Carlson, C., Carrasco, G.,
620   Casacuberta, N., Casciotti, K. L., Castrillejo, M., Chamizo, E., Chance, R., Charette, M. A.,
621   Chaves, J. E., Cheng, H., Chever, F., Christl, M., Church, T. M., Closset, I., Colman, A., Conway,
622   T. M., Cossa, D., Croot, P., Cullen, J. T., Cutter, G. A., Daniels, C., Dehairs, F., Deng, F., Dieu, H.
623   T., Duggan, B., Dulaquais, G., Dumousseaud, C., Echegoyen-Sanz, Y., Edwards, R. L., Ellwood,
624   M., Fahrbach, E., Fitzsimmons, J. N., Russell Flegal, A., Fleisher, M. Q., van de Flierdt, T.,
625   Frank, M., Friedrich, J., Fripiat, F., Fröllje, H., Galer, S. J. G., Gamo, T., Ganeshram, R. S., Garcia-
626   Orellana, J., Garcia-Solsona, E., Gault-Ringold, M., et al.: The GEOTRACES Intermediate Data
627   Product 2017, Chem. Geol., doi:10.1016/j.chemgeo.2018.05.040, 2018.

628   Sigman, D. M. and Casciotti, K. L.: Nitrogen Isotopes in the Ocean, in Encyclopedia of Ocean
629   Science, pp. 1884–1894, Academic Press., 2001.

630   Sigman, D. M., Altabet, M. A., Francois, R., McCorkle, D. C. and Gaillard, J. F.: The isotopic
631   composition of diatom-bound nitrogen in Southern Ocean sediments, Paleoceanography,
632   14(2), 118–134, 1999.

633 Sigman, D. M., DiFiore, P. J., Hain, M. P., Deutsch, C. and Karl, D. M.: Sinking organic matter
634 spreads the nitrogen isotope signal of pelagic denitrification in the North Pacific, Geophys.
635 Res. Lett., 36, doi:10.1029/2008gl035784, 2009.

636 Somes, C. J., Schmittner, A. and Altabet, M. A.: Nitrogen isotope simulations show the
637 importance of atmospheric iron deposition for nitrogen fixation across the Pacific Ocean,
638 Geophys. Res. Lett., 37, doi:10.1029/2010gl044537, 2010.

639 Tawa, A., Ishihara, T., Uematsu, Y., Ono, T. and Ohshimo, S.: Evidence of westward
640 transoceanic migration of Pacific bluefin tuna in the Sea of Japan based on stable isotope
641 analysis, Mar. Biol., 164(4), doi:10.1007/s00227-017-3127-8, 2017.

642 Thimm, G. and Fiesler, E.: Optimal Setting of Weights, Learning Rate, and Gain, , 15, 1997.

643 Thunell, R. C., Sigman, D. M., Muller-Karger, F., Astor, Y. and Varela, R.: Nitrogen isotope
644 dynamics of the Cariaco Basin, Venezuela, Glob. Biogeochem. Cycles, 18(3),
645 doi:10.1029/2003gb002185, 2004.

646 Toggweiler, J. R. and Carson, S.: What Are Upwelling Systems Contributing to the Ocean's
647 Carbon and Nutrient Budgets?, in Upwellmg in the Ocean: Modern Processes and Ancient
648 Records, edited by K.-C. . meis C.P. Summerhayes M. V. Angel, R. L. Smith, and B. Zeiizschcl,
649 John Wiley & Sons Ltd., 1995.

650 Toggweiler, J. R., Dixon, K. and Broecker, W. S.: The Peru upwelling and the ventilation of
651 the South-Pacific thermocline, J. Geophys. Res.-Oceans, 96(C11), 20467–20497,
652 doi:10.1029/91jc02063, 1991.

653 Trull, T. W., Davies, D. and Casciotti, K.: Insights into nutrient assimilation and export in
654 naturally iron-fertilized waters of the Southern Ocean from nitrogen, carbon and oxygen
655 isotopes, Deep Sea Res. Part II Top. Stud. Oceanogr., 55(5–7), 820–840,
656 doi:10.1016/j.dsr2.2007.12.035, 2008.

657 Tuerena, R. E., Ganeshram, R. S., Geibert, W., Fallick, A. E., Dougans, J., Tait, A., Henley, S. F.
658 and Woodward, E. M. S.: Nutrient cycling in the Atlantic basin: The evolution of nitrate
659 isotope signatures in water masses, Glob. Biogeochem. Cycles, 29(10), 1830–1844,
660 doi:10.1002/2015GB005164, 2015.

661 Wada, E. and Hattori, A.: Nitrogen isotope effects in the assimilation of inorganic
662 nitrogenous compounds by marine diatoms, Geomicrobiol. J., 1(1), 85–101, 1978.

663 Yang, S. and Gruber, N.: The anthropogenic perturbation of the marine nitrogen cycle by
664 atmospheric deposition: Nitrogen cycle feedbacks and the [15] N Haber-Bosch effect, Glob.
665 Biogeochem. Cycles, 30(10), 1418–1440, doi:10.1002/2016GB005421, 2016.

666 Yang, S., Gruber, N., Long, M. C. and Vogt, M.: ENSO-Driven Variability of Denitrification and
667 Suboxia in the Eastern Tropical Pacific Ocean, Glob. Biogeochem. Cycles, 31(10), 1470–
668 1487, doi:10.1002/2016GB005596, 2017.

Biogeosciences
Discussions

Open Access

EGU

669   Yoshikawa, C., Makabe, A., Shiozaki, T., Toyoda, S., Yoshida, O., Furuya, K. and Yoshida, N.:
670   Nitrogen isotope ratios of nitrate and N* anomalies in the subtropical South Pacific,
671   Geochem. Geophys. Geosystems, 16(5), 1439–1448, doi:10.1002/2014GC005678, 2015.
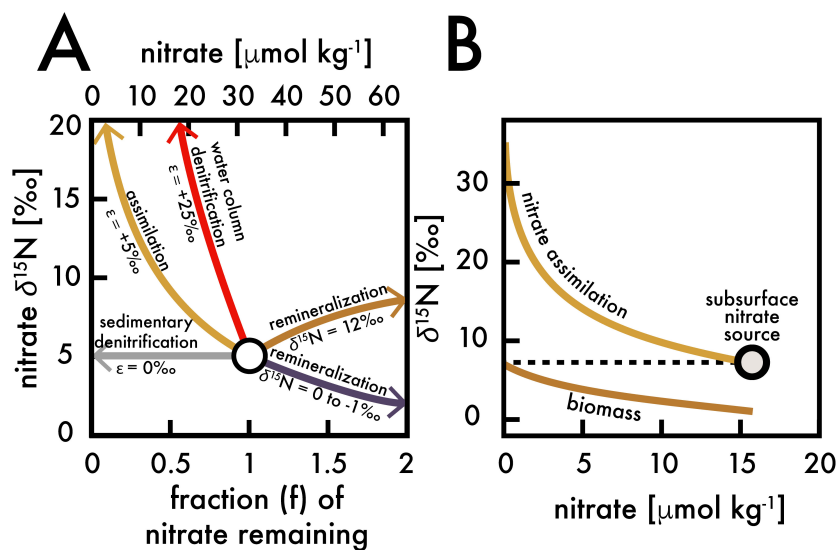
Figure 1: (A) A comparison of influences on average deep-sea nitrate (circle; concentration and $\delta^{15}N$ estimated here by EANN results in this work) including: the isotope effects of assimilation (yellow arrow), water column and sedimentary denitrification (red and gray arrows), and the addition of nitrate via remineralization of organic matter with higher and lower $\delta^{15}N$ (brown and purple arrows) (modified from Galbraith et al., (2008)). (B) An example of N isotopic fractionation on nitrate and organic matter biomass during nitrate assimilation in eastern equatorial Pacific surface waters (from Rafter and Sigman, (2016)). These calculations are based on isotopic fractionation equations of (Mariotti et al., 1981) simplified in (Sigman and Casciotti, 2001) with an isotope effect (ε) as shown in (A). The variable "f" is the observed / initial nitrate concentration.
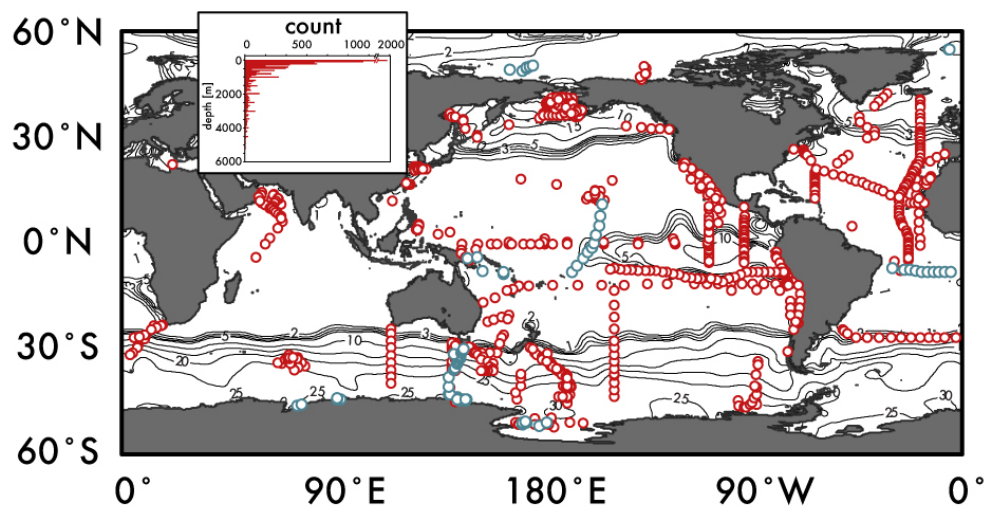
Figure 2: The location of global nitrate δ^{15}N observations used to constrain the Ensemble of Artificial Neural Networks are shown as red circles. Observations used as an 'external validation dataset' (those withheld from training the EANN) are shown in blue. Inset figure shows the number of observations versus depth. Contours are surface nitrate concentrations for October-December from World Ocean Atlas (Garcia et al., 2014).
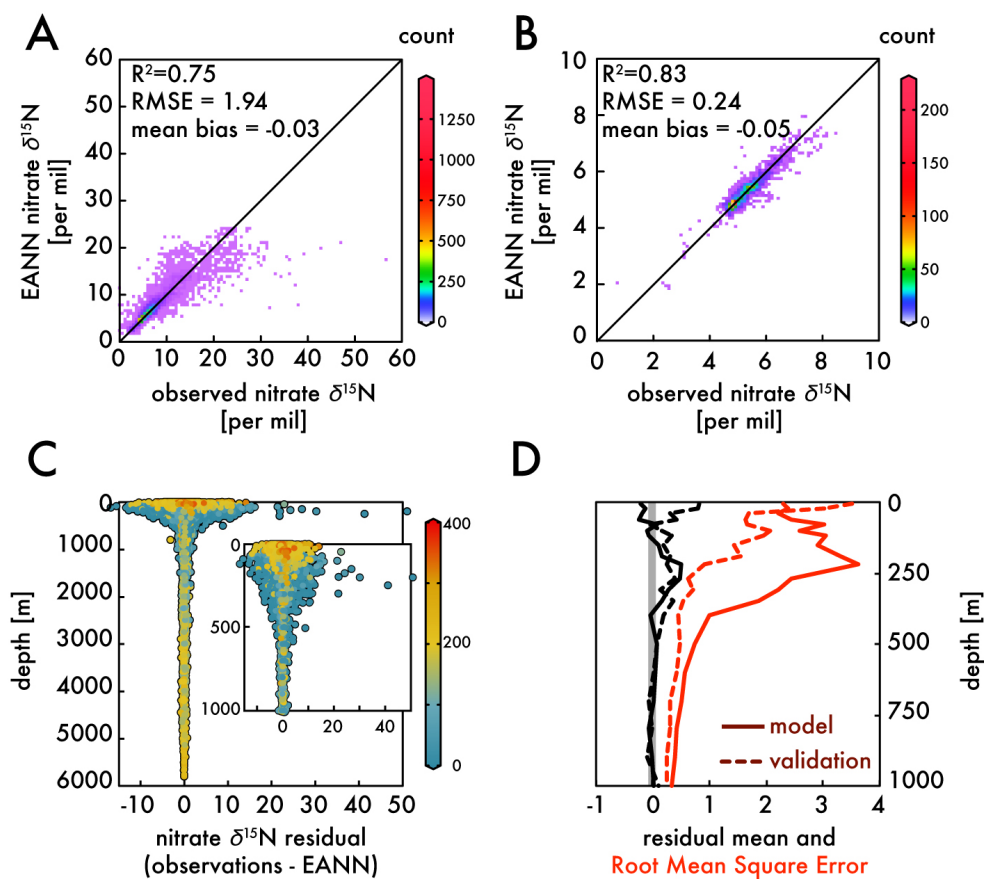
Figure 3: The binned observed versus EANN-predicted nitrate δ^{15}N are shown for all depths in (A) and for >1000 m in (B). The colors indicate the number of comparisons on the World Ocean Atlas grid. The anomalously high observed nitrate δ^{15}N values (>30‰) in (A) are exclusively from the Eastern Tropical South Pacific waters (Bourbonnais et al., 2015; Casciotti et al., 2013; Rafter et al., 2012; Ryabenko et al., 2012). The difference (or residual) between the observations and EANN nitrate δ^{15}N is made for all depths and the upper 1000 m in (C) with colors representing the dissolved oxygen content. Note the largest offsets between 100-500 m in (C) are associated with lowest oxygen content. Similarly, the mean residual (black) and Root Mean Square Error (RMSE; red) with depth (D) are highest in the upper 500 m. Dashed lines in (D) demonstrate the same statistics, but for the external validation dataset (blue in Fig. 2).
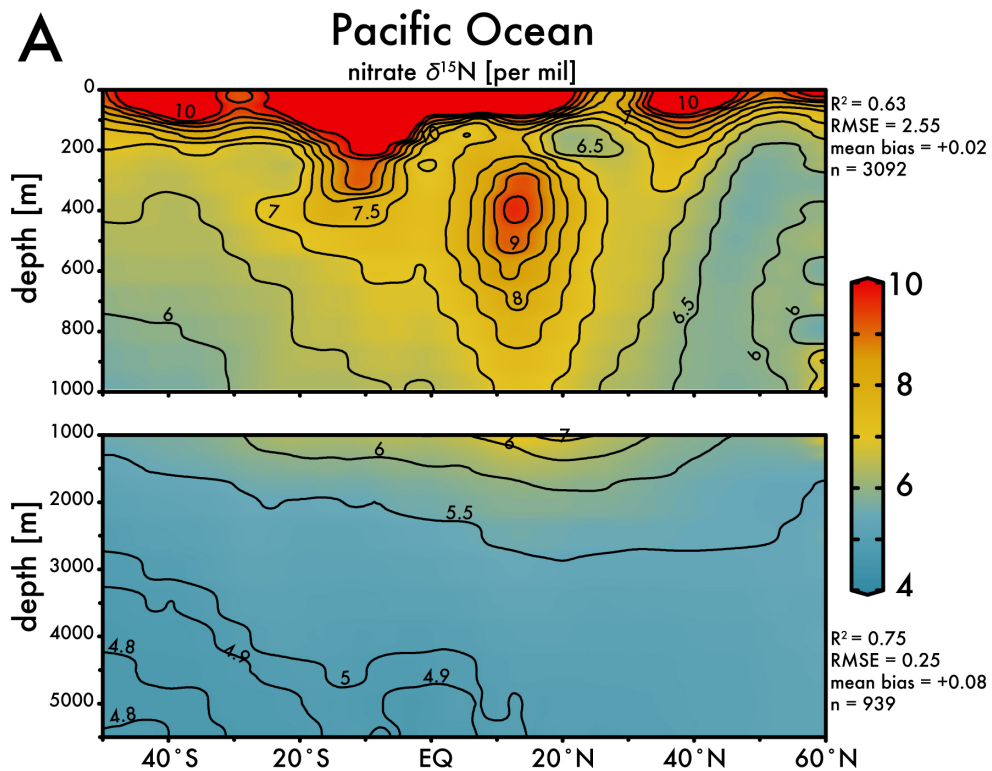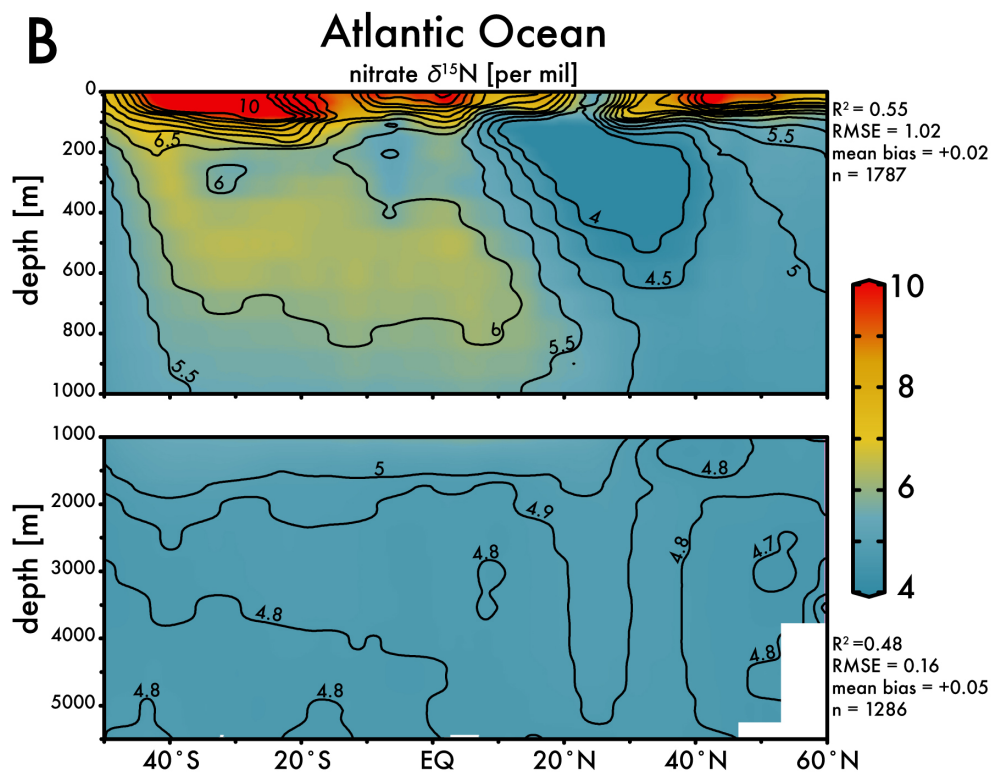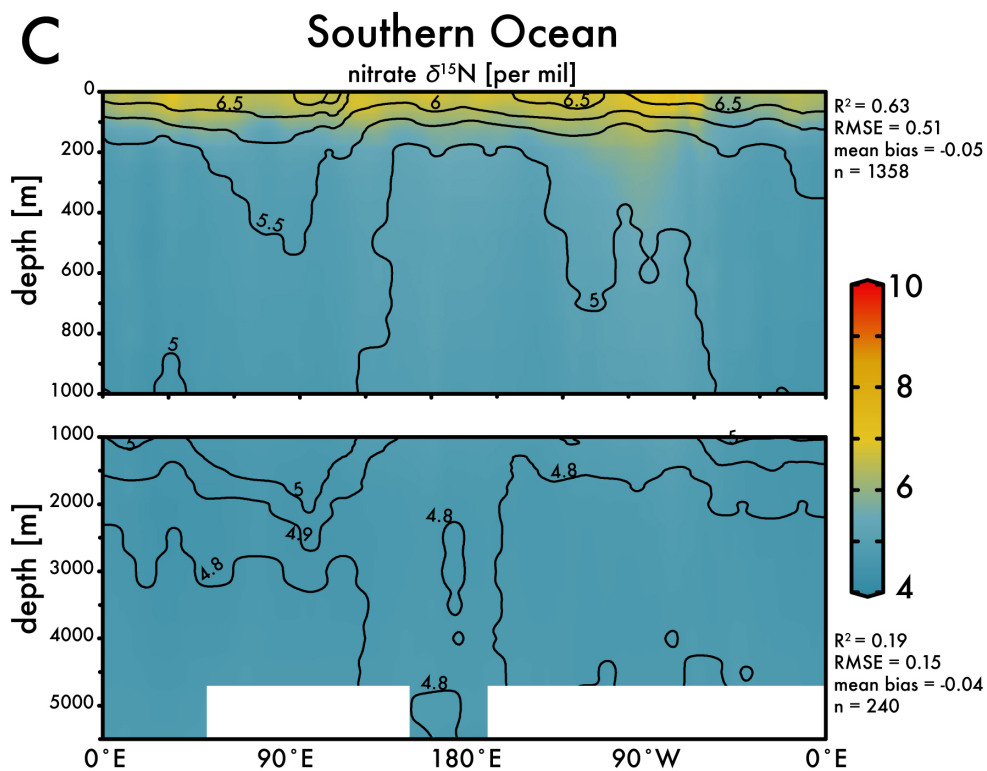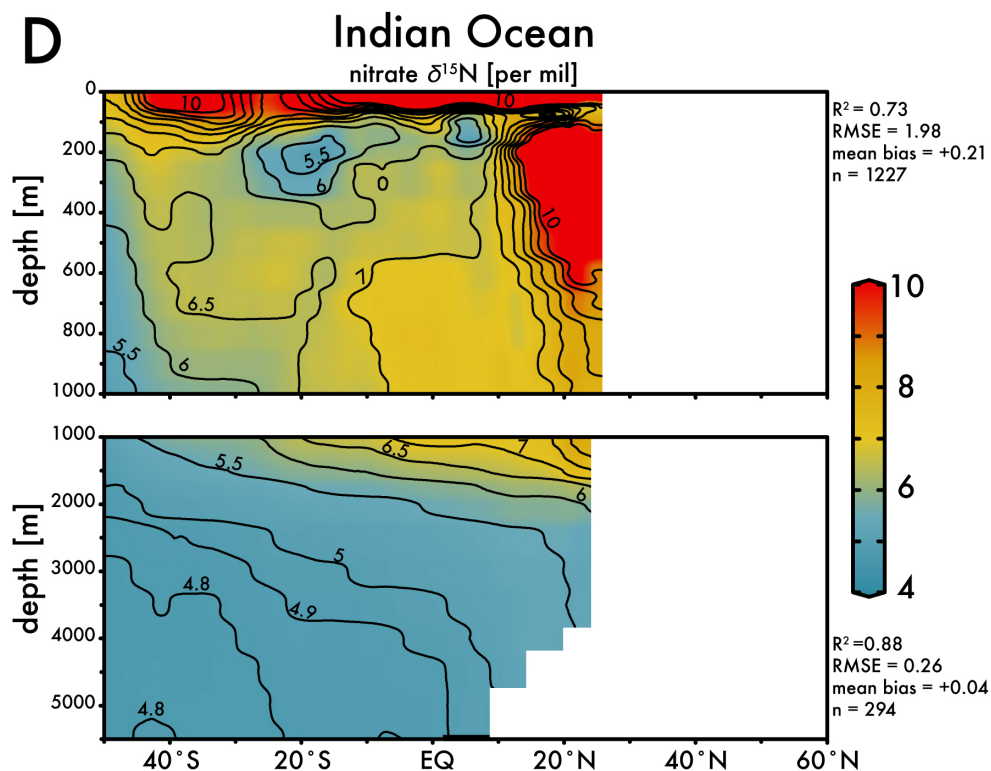
**Figure 4**: Zonal average of model nitrate δ^{15}N versus latitude or longitude for the: (A) Pacific Ocean, (B) Atlantic Ocean, (C) Southern Ocean, and the (D) Indian Ocean. White bars indicate no data because of land. The R^2, RMSE, mean bias, and total number (n) of observed versus EANN nitrate δ^{15}N are shown on the right for each region and depth range. White indicates regions of no data coverage.
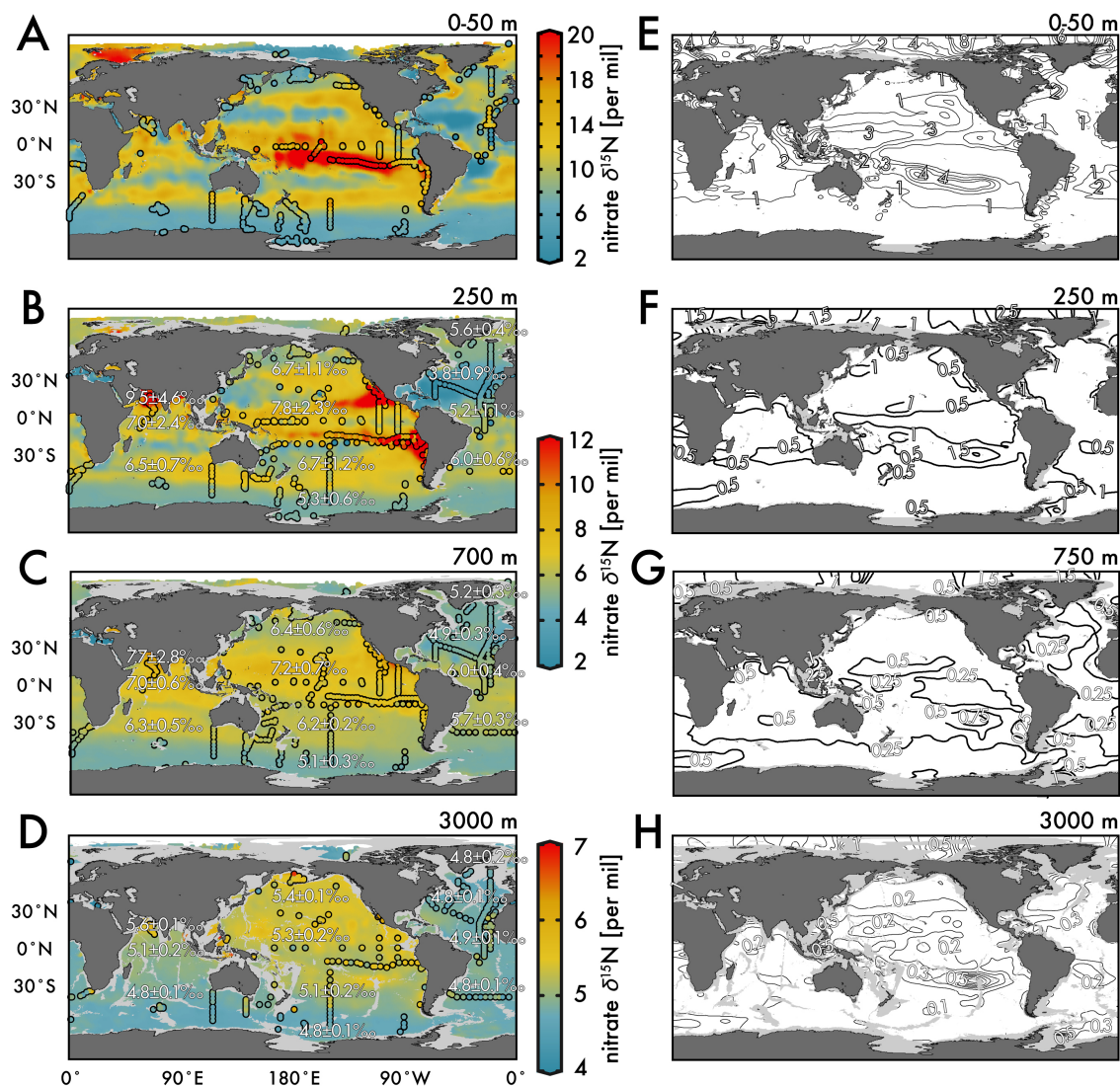
Figure 5: (Left) Map view of nitrate δ^{15}N from our EANN and our observations (circles) for the (A) average over the 0-50 m depth as well as the (B) 250 m, (C) 700 m, and (D) 3000 depth surfaces. Numbers are average model nitrate δ^{15}N for that basin, depth, and latitude. (Right) Map views of nitrate δ^{15}N error from the EANN model nitrate δ^{15}N for the same depth surfaces on left.
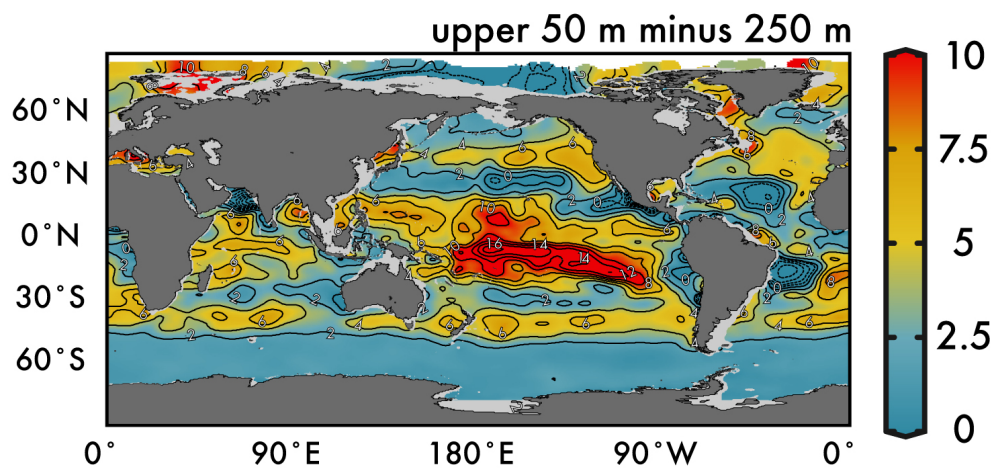
Figure 6: Difference between the average nitrate δ^{15}N in the upper 50m and 250 m depths in Figure 5. Dashed contours in low latitude ODZ regions and subtropical gyres indicate regions where nitrate δ^{15}N at 250 m is greater than the upper 50 m nitrate δ^{15}N.

Biogeosciences
Discussions

Open Access

EGU
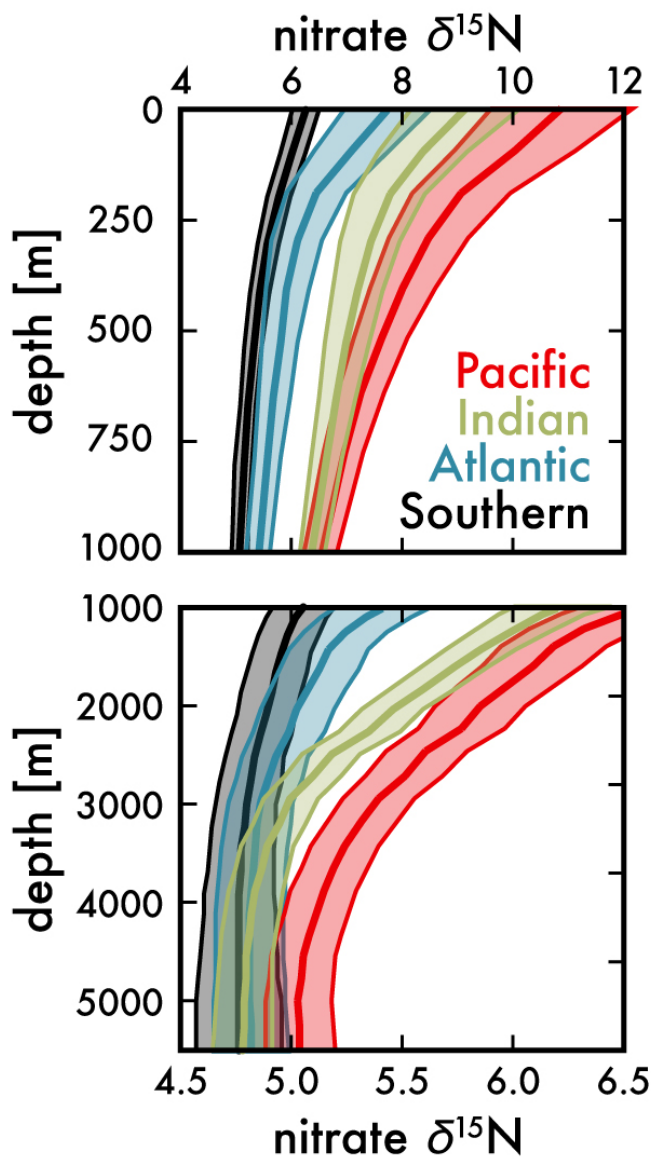
Figure 7: Mean EANN nitrate $\delta^{15}N$ (solid line) and 1-sigma standard deviation (envelope) with depth for each ocean basin. Note change in vertical and horizontal axes between top and bottom.

Biogeosciences
Discussions

Open Access

EGU

Appendix: References for this version of seawater nitrate $\delta^{15}N$ compilation

region	year of sampling	month of sampling	reference
Pacific North – Subarctic	Unknown sampling date	*na*	(Altabet and Francois, 1994)
Indian – Arabian Sea	1995	8	(Altabet et al., 1999)
Southern Ocean - Pacific	1996-1998	1-4,8-11	(Altabet and Francois, 2001)
Pacific North – Gulf of California	1990	6	(Altabet, 1999)
Pacific North – Subarctic	1971	7	(Wada, 1980)
Indian – Arabian Sea	1994	4	(Brandes et al., 1998)
Pacific North – ETNP	1993	12	(Brandes et al., 1998)
Pacific North - Kuroshio	1992 & 1994	3 & 4	(Liu et al., 1996)
Pacific North – Tropical	1997	10 & 11	(Voss et al., 2001)
Pacific North – Subarctic	2003	2	(Galbraith, 2007)
Atlantic North	2004	5	(Bourbonnais et al., 2009)
Mediterranean	1996	5	(Sachs, 1999)
Mediterranean	1998	1	(Pantoja et al., 2002)
Pacific North – Subarctic	2002	6	(Lehmann et al., 2005)
Pacific South – Tropical	1977	6	(Liu, 1979)
Pacific South – Tropical	2002 & 2004	4 & 5	(De Pol-Holz et al., 2009)
Pacific North – Okhotsk	1998, 1999, 2000	6 & 9	(Yoshikawa et al., 2006)
Pacific Tropical	2006	6	(Kienast et al., 2008)
Southern Ocean – Indian	2005	1 & 2	(Trull et al., 2008)
Pacific South – Tropical	2008 & 2009	1, 2, & 12	(Ryabenko et al., 2012)
Indian South	2011	10 & 11	(Dehairs et al., 2015)
Pacific South – Tropical	2012	11	(Bourbonnais et al., 2015)
Indian North	2007	9	(Gaye et al., 2013)
Atlantic South	2010 & 2012	10 & 1	(Tuerena et al., 2015)
Pacific South	2009	6	(Yoshikawa et al., 2015)

Biogeosciences Open Access
Discussions

EGU

Pacific North –SCS	1997	4	(Wong et al., 2002)
Pacific North – Bering Sea	2008 & 2007	4 & 5	(Granger et al., 2011, 2013)
Arctic – Beaufort	2009	9	Granger unpublished
Atlantic North	2010	10 & 11	Jenkins et al. Unpublished GEOTRACES (Knorr_199_leg4.pdf)
Atlantic Tropical	2010	2 & 3	Frank et al. Unpublished GEOTRACES (meteor81_1.pdf)
Pacific Tropical	2013	5 & 6	(Lehmann et al., 2018)
Pacific North	2008	7	Granger Unpublished
Pacific North	2009 & 2011	2 & 7	(Umezawa et al., 2014)
Pacific South – Tropical	2010 & 2011	2-4	(Knapp et al., 2016)
Atlantic North – Subarctic	1989	6	(Voss, 1991)
Southern Ocean – Pacific	1995	4	(Sigman et al., 1999)
Southern Ocean – Indian	1995	1	(Sigman et al., 1999)
Southern Ocean – Pacific	2016		(Kemeny et al., 2016)
Pacific North – Tropical	2003	10	(Sigman et al., 2005)
Pacific North – ALOHA	2000	11	(Sigman et al., 2009)
Atlantic – North	2001-2002	1-12	(Knapp et al., 2005)
Atlantic – North	2002	10	(Knapp et al., 2008)
Pacific – North	2003	7 & 8	(Knapp et al., 2011)
Indian - South	1999	1 & 2	(Karsh et al., 2003)
Southern – Indian	1998 & 1999	2,3,4,9, & 12	(DiFiore et al., 2006)
Southern – Atlantic	2012	7	(Smart et al., 2015)
Atlantic – North	2011	10 & 11	(Marconi et al., 2015)
Pacific – North ALOHA	2004	7	(Casciotti et al., 2008)
Pacific – South Tropical	2005	11	(Casciotti et al., 2013)
Pacific – North Tropical	2003	11	(Casciotti and McIlvin, 2007)
Indian – Arabian	2007	9	(Martin and Casciotti, 2017)
Pacific – Tropical	2004-2007	3-12	(Rafter et al., 2012; Rafter and Sigman, 2016)

Indian – Arabian Sea	2007	10	(DeVries et al., 2012) or Rafter and Sigman Unpublished
Pacific South – Tasman Sea	2010	1 & 2	Rafter and Sigman Unpublished
Pacific South – Tropical	2010	2	(Rafter et al., 2012)
Atlantic North – Subarctic	2010	4	Rafter and Sigman Unpublished
Pacific South	2005	1	(Rafter et al., 2013)
Pacific South – Tropical	2013	10-12	(Peters et al., 2017)
Atlantic North – Subarctic	2013	8	(Marconi et al., 2017)
Pacific North – Subarctic	1993	5	(Wu et al., 1997)
Arctic	2014	7 & 8	(Fripiat et al., 2018)